PAPER

Preparation of a Pt/TiO₂/cotton fiber composite catalyst with low air resistance for efficient formaldehyde oxidation at room temperature†

Longhui Nie, [ID] *[a] Jie Wang[a] and Jiaguo Yu [ID] *[b]

For the first time, nano TiO₂ was coated on the surface of cotton fiber by a dip-coating method, and then Pt nanoparticles (NPs) were deposited onto the surface of the TiO₂/cotton fiber (TC) to obtain a Pt/TiO₂/cotton fiber composite (PTC) catalyst by a combined method involving the impregnation of the TiO₂/cotton fiber with the Pt precursor and NaBH₄-reduction. The prepared PTC sample was used for oxidative decomposition of formaldehyde (HCHO) at room temperature and the effect of Pt loading on catalytic performance was investigated. The results show that the PTC catalyst has much lower air resistance than the powder-like sample, which is of great importance for its actual application, and it can efficiently catalyze oxidation of HCHO into CO₂ and H₂O. The optimum Pt loading was 0.75 wt%. The PTC catalyst also exhibited good catalytic stability in recycling experiments. The TiO₂ coating in the PTC catalysts plays an important role in obtaining a high catalytic activity and a good stability. *In situ* diffuse reflectance infrared Fourier transformation spectroscopy (DRIFTS) results showed that formate, CO and dioxymethylene (DOM) species are the main intermediate species, and a mechanism for HCHO catalytic oxidation over the PTC catalyst was proposed. This work may promote the actual application of high-performance catalysts for indoor air purification and related catalytic processes due to the merits of low air resistance, light mass, flexible properties, good efficiency of the PTC catalyst, and low cost, as well as cotton being an abundant raw material.

1. Introduction

Because human beings spend most of their time indoors, the quality of indoor air is vital to human health. Formaldehyde (HCHO) is a major indoor pollutant and may cause many health problems, such as eye and skin irritation, nasal tumors, and nasopharyngeal cancer and so on, when people are exposed to air containing-HCHO for a long time.[1–3] To purify indoor air, many strategies, including adsorption,[4–8] photocatalytic oxidation,[9,10] plasma technology,[11] thermal catalytic oxidation[12–20] and so on, have been adopted to eliminate HCHO in the air. Among them, thermal catalytic oxidation of HCHO into CO₂ and H₂O at ambient temperature has attracted much attention due to its merits of being environmentally friendly and energy saving.[2,12–17] For the catalytic oxidation of HCHO at room temperature, metal oxides (such as MnO₂ [21–23]) and supported noble metal catalysts have been widely investigated by many

groups.[12,14–18,24–27] Zhang *et al.*[25] for the first time discovered that HCHO could be catalytically oxidized into CO₂ and H₂O on the supported noble metal (Pt, Rh, Pd and Au) catalysts at ambient temperature. Huang *et al.*[15,28] developed an impregnation and NaBH₄ reduction approach to prepare supported noble metal catalysts (Pt/TiO₂, Pd/TiO₂) which could efficiently oxidize HCHO into CO₂ and H₂O at room temperature. Our previous work also showed that HCHO could be completely decomposed into CO₂ and H₂O over supported Pt catalysts by an impregnation and NaOH-assisted NaBH₄ reduction combined method.[24,29,30] In the aforementioned catalysts, the supported Pt catalyst revealed better catalytic activity for HCHO oxidation than other catalysts at room temperature. However, most of metal oxide and supported noble metal catalysts were synthesized in powder form, which makes many problems in practical applications, such as bringing the possibility of high air resistance, needing to be pressed into tablets or attached to other big-block supports in use. In order to overcome the drawbacks, we attempted to use the inorganic TiO₂ nanofiber by electrospinning[31] and honeycomb ceramics (HC)[32] as supports to prepare the supported Pt/TiO₂ and Pt/HC catalysts. But, the brittle property for the former and the big mass for the latter hinder their actual applications in air purifier. Therefore, it is highly desired to develop a robust, flexible and light-mass, low-air-resistance and highly-efficient catalyst for air purifier. The organic and inorganic composite catalyst may be a good choice

[a]School of Materials and Chemical Engineering, Hubei University of Technology, Wuhan 430068, China. E-mail: nielonghui@mail.hbut.edu.cn

[b]State Key Laboratory of Advanced Technology for Materials Synthesis and Processing, Wuhan University of Technology, Wuhan 430070, China. E-mail: jiaguoyu@yahoo.com

and has received much attention in the field of photocatalytic self-cleaning and antibacterial in recent years.[33–38]

However, up to date, few attempts have been made to develop such organic and inorganic composite catalyst for room-temperature catalytic oxidation of HCHO in indoor air. Here, we for the first time report the preparation of the Pt/TiO₂/cotton fiber composite catalysts and their use for catalytic oxidation of HCHO in air at room temperature. The obtained PTC catalysts show low air resistance, good catalytic performance and stability.

2. Experimental

All reagents used in this work were purchased with analytical grade and directly used without further purification.

2.1 Preparation of TiO₂ nanosol

Titania nanosol was synthesized by a hydrolysis method at room temperature using titanium(IV) butoxide (Sinopharm Chemical Reagent Co., Ltd) as the precursor. In a typical procedure, 10 mL of titanium(IV) butoxide was dissolved in 25 mL of ethanol. The resulted solution was added dropwise to 200 mL of 0.04 M nitric acid solution under stirring at room temperature and kept stirring for 6 days to form the uniform and stable TiO₂ nanosol.

2.2 Coating TiO₂ on the surface of cotton fiber

The commercial absorbent cotton was used as the support because of its low cost, abundant raw material, light mass, and flexible properties. The coating process of TiO₂ on the surface of cotton fiber was as follows: the absorbent cotton was firstly immersed in TiO₂ nanosol for 5 min, and then taken out and pressed between two pieces of filter paper to remove the excess of liquid. The resulted product was dried in an oven at 60 °C for 5 min and then at 115 °C for 30 min. Finally, the obtained sample was rinsed twice (each for 5 min) with the deionized water and dried at 60 °C overnight to obtain the TiO₂/cotton fiber composite, which denoted as TC.

2.3 Preparation of Pt/TiO₂/cotton fiber composite catalyst

In a typical synthesis, the obtained TC in above process was immersed in 10 mL of chloroplatinic acid aqueous solution, and kept shaking for 30 min. After that, the mixture (2.5 mL) of NaOH (0.5 M) and NaBH₄ (0.1 M) solutions was added into the above solution quickly and kept shaking for 10 min. Finally, the resulted product was separated from the solution and then dried at 60 °C overnight. The nominal weight of Pt to support was 0.1, 0.25, 0.5, 0.75, 1 wt%, respectively. The corresponding samples are denoted as PTC0.1, PTC0.25, PTC0.5, PTC0.75, and PTC1.0. The real content of Pt determined by inductively coupled plasma atomic emission spectroscopy (ICP-AES) was 0.05, 0.14, 0.25, 0.36, and 0.46 wt% for the PTC0.1, PTC0.25, PTC0.5, PTC0.75, and PTC1.0 samples, respectively (shown in Table 1).

Table 1 The basic parameters for the as-synthesized samples

Samples	S_{BET} (m² g⁻¹)	V_{pore} (cm³ g⁻¹)	d_{pore} (nm)	Pt wt% by ICP-AES
Cotton	26.5	0.020	3.0	—
TC	16.4	0.018	4.51	—
PC0.5	3.6	0.009	10.2	0.25
PTC0.1	18.4	0.021	4.61	0.05
PTC0.25	17.5	0.020	4.63	0.14
PTC0.5	10.7	0.015	5.82	0.25
PTC0.75	7.2	0.012	6.12	0.36
PTC1.0	4.9	0.008	7.14	0.46

For comparison, the 0.5 wt% Pt/cotton catalyst was also prepared using cotton as support directly, which is denoted as PC0.5. The real content of Pt was 0.25 wt% for the PC0.5 sample.

2.4 Characterization

The crystal phase composition of the samples was analyzed by a D8 X-ray diffractometer (Bruker) with Cu K$_\alpha$ radiation at a scan rate (2θ) of 0.05° s⁻¹. Transmission electron microscopy (TEM) and high-resolution transmission electron microscopy (HRTEM) images were obtained on a Tecnai G2 F20 microscope at an accelerating voltage of 200 kV. X-ray photoelectron spectroscopy (XPS) studies were performed on VG ESCALAB250xi with X-ray monochromatisation. The C 1s peak at 284.6 eV of the surface adventitious carbon was used as a reference for all binding energies (BE). The Brunauer–Emmett–Teller (BET) surface area (S_{BET}) of the samples was acquired from nitrogen adsorption data recorded on a Micromeritics ASAP 3020 nitrogen adsorption apparatus (USA). All the samples were degassed at 120 °C before nitrogen adsorption measurements. The BET surface area was calculated from the adsorption data by a multipoint method in the relative pressure range of $P/P_0 = 0.05$–0.3. The pore size distributions were determined using adsorption isotherms by the Barrett–Joyner–Halenda (BJH) method, and supposing a cylindrical pore model. The single point nitrogen adsorption total pore volume at the relative pressure of $P/P_0 = 0.99$ was used to determine the pore volume and average pore size.

In situ diffuse reflectance infrared Fourier transformations spectroscopy measurement was carried out on a Thermo Fisher 6700 instrument. The catalyst was pretreated at 120 °C for 2 h under a gas flow of dried air *in situ* cell reactor. After that, the reactant gas mixture (80 ppm of HCHO + O₂) was introduced into the DRIFTS cell at room temperature by a mass flow controller with a flow rate of 30 mL min⁻¹. All spectra were obtained after subtracting the background. Scans were collected from 4000 to 650 cm⁻¹ with a resolution of 4 cm⁻¹.

2.5 Air resistance experiment

Air resistance experiment was carried out in a home-made setup, as shown in Fig. 1. The PTC or TC sample (18 mg) was loaded and kept tight (volume: 0.31 cm³) in a tube (inner diameter: 6 mm) with its outlet connected to air and its inlet connected with a precision digital pressure gauge (DP-AF, Sanli
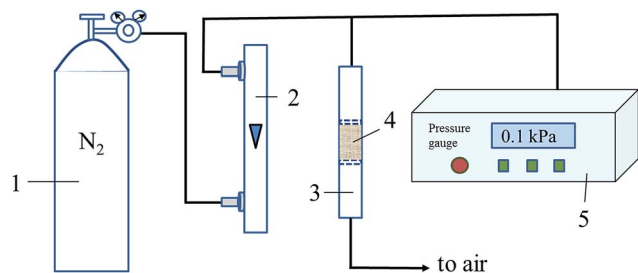
Fig. 1 Schematic diagram for measuring air resistance of the samples. (Here, (1) N_2 cylinder; (2) rotor flowmeter; (3) sample tube; (4) sample; (5) precision digital pressure gauge).

Electronics). The pressure gauge can detect and reveal the pressure difference between the pressure in the pipe before inlet of tube and the atmospheric pressure outside. N_2 flow (120 mL min^{-1}) was introduced into the tube with sample inside. The readings on the pressure gauge are used to evaluate the magnitude of air resistance of the samples. The bigger reading on the pressure gauge will be when the higher air resistance of the sample is. As a comparison, the powder-like Pt/TiO_2 (P25, Degussa) sample (prepared in the same way with literature[24]) with the same volume or the same mass with PTC was used for air resistance test in the same way, and the corresponding measured pressure differences are presented as Δp_{volume} and Δp_{mass}, respectively.

2.6 Catalytic activity evaluation

The HCHO catalytic oxidation test was performed under a dark condition at 20 °C and 50–60% relative humidity in the same way as it is reported in our previous work.[24,29] 0.3 g of catalyst was used to evaluate the catalytic activity of the prepared samples and HCHO initial concentration was kept about 150 ppm. A Photoacoustic IR Multigas Monitor (INNOVA air Tech Instruments Model 1412) was used to on-line monitor the HCHO and CO_2 concentrations. The time for each set of experiment was fixed to be 60 min. The HCHO concentration decrease and CO_2 concentration increase (ΔCO_2, which is the difference of CO_2 concentration at t reaction time and at initial time, ppm) were used to evaluate the catalytic performance.

3. Results and discussion

3.1 Results of air resistance measurement

The results of air resistance experiment for the as-prepared samples are shown in Table 2. When the PC and PTC sample

Table 2 Results of air resistance experiment for the as-synesized samples

Samples	Δp_{volume} (kPa)	Δp_{mass} (kPa)
TC	0.15	
PTC1.0	0.11	
Pt/TiO_2	30.75	8.88

were loaded in the tube, the pressure differences are 0.15 and 0.11 kPa, respectively. However, when the powder-like Pt/TiO_2 sample was loaded in the tube, the pressure differences are 8.88 and 30.75 kPa for the powder-like Pt/TiO_2 sample with the same mass and the same volume as PTC, respectively, indicating that much lower air resistance for the TC and PTC samples and much higher air resistance for the powder-like Pt/TiO_2 sample. The much lower air resistance for the PTC sample (similar to TC) is due to the large number of macropores existing among the cotton fibers and facilitating gas flow through (see Fig. 2), which is of great importance for the application of the catalyst in air purifier.

3.2 Phase structures, morphology and element composition

The phase structures of cotton before and after coating TiO_2 as well as depositing Pt NPs on its surface were investigated by X-ray diffraction (XRD) with the diffraction angle (2θ) in the range 20–80 °C. The XRD patterns of the cotton, PC and PTC1.0 samples are shown in Fig. 3. From the Fig. 3, it reveals that two peaks located at $ca.$ 23° and 34° belong to the typical characteristic peaks of cellulose fibers.[33,34] No TiO_2 peaks (such as: most intensive peak located at 25.3° for anatase and 28.4° for rutile, respectively) can be observed for the TC and PTC1.0 samples, indicating that most of TiO_2 on the surface of cotton are amorphous, which is mainly due to the hydrolysis process taking place under the room temperature. At the same time, no Pt characteristic peaks also can be observed in the XRD pattern of the PTC1.0 sample, which may be due to the low content, small size and good dispersion of Pt NPs.[24,29]

The typical surface morphology of cotton before and after coating TiO_2 as well as depositing Pt NPs was observed by FESEM, as shown in Fig. 4. Fig. 4a and b show the typical morphology of crude cotton, indicating the surface of crude cotton is rather rough. After deposition TiO_2, the TiO_2 coating can be clearly observed and the surface of cotton becomes smooth (shown in Fig. 4c and d), indicating very small TiO_2 NPs was formed in the sol by the hydrolysis method. Further depositing Pt NPs, the surface of TC doesn't show an obvious change (see Fig. 4e and f). The morphology and particle size of TiO_2 and Pt NPs were further observed by TEM (see Fig. 5a–c) and HRTEM images (see Fig. 5d). Fig. 5a shows the typical
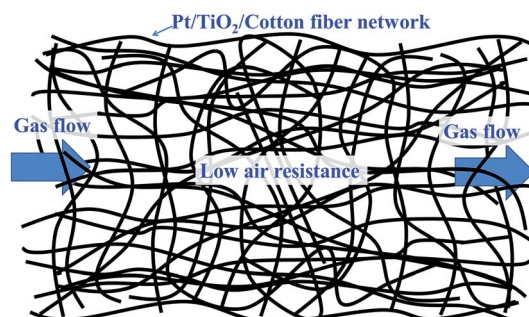

Fig. 2 Schematic diagram for gas flow through porous Pt/TiO_2/cotton fiber network.
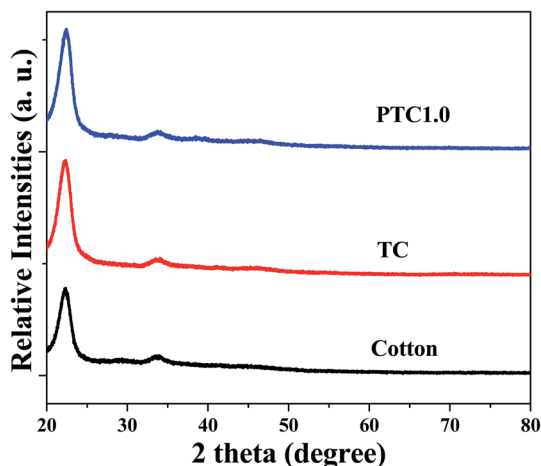
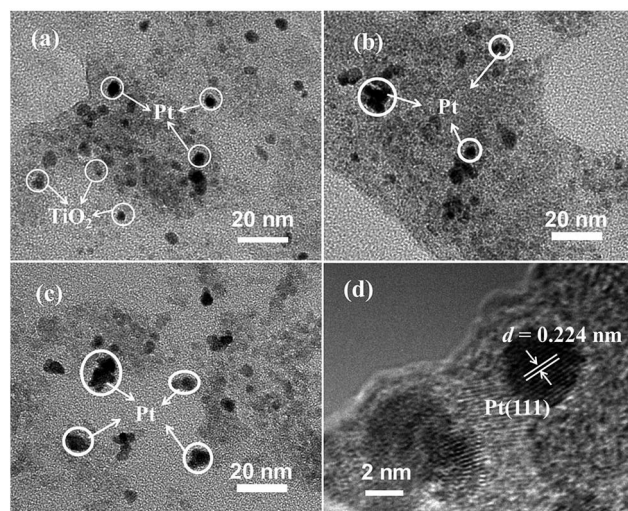Fig. 3 XRD patterns of the cotton, PC and PTC1.0 samples.

Fig. 4 Typical SEM images of the cotton fiber (a, b), TC (c, d) and PTC1.0 (e, f) samples.

Fig. 5 Typical TEM images of the PTC0.25 (a), PTC0.5 (b) and PTC1.0 (c) samples, and HRTEM image (d) of the PTC0.25 sample.
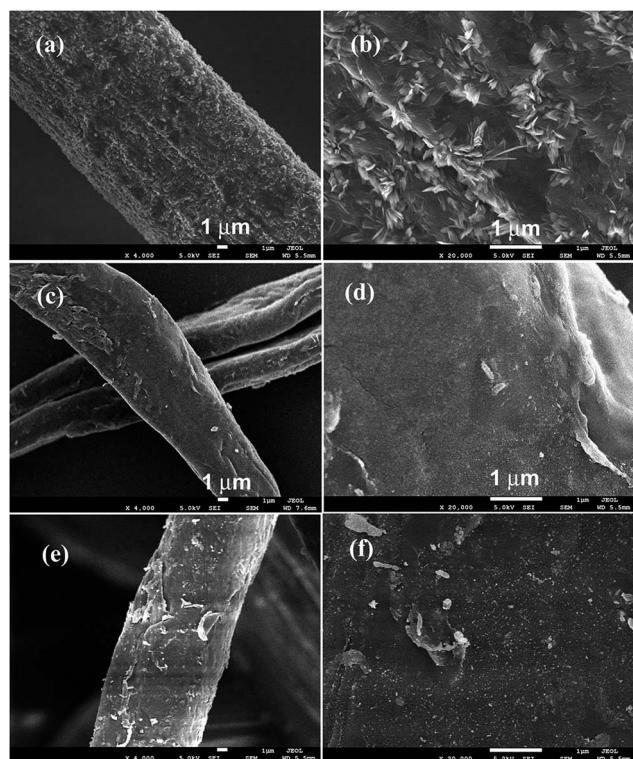
3.3 Nitrogen adsorption

The N_2 adsorption–desorption isotherms and corresponding pore size distribution curves of the TC, PTC0.5 and PTC1.0 samples were plotted in Fig. 6. The N_2 adsorption–desorption isotherms (shown in Fig. 6a) of the above three samples are of type IV according to the classification of IUPAC (International Union of Pure and Applied Chemistry),[39] suggesting the existence of mesopores. With increasing the Pt content from 0 wt% to 1.0 wt%, the isotherms of the PC, PTC0.5 and PTC1.0 samples go downwards obviously, indicating an obvious decrease of the specific surface area for above three samples with the increase of Pt content. Also, the hysteresis loops for the three samples are like H3 type for at a high relative pressure range between 0.4 and 1.0, which also suggests the existence of mesoporous pore. The pore-size distribution curves (shown in Fig. 6b) obtained from the adsorption branch of the isotherms further reveal the existence of mesopores. A wide pore size distribution (2–100 nm) is found for the TC, PTC0.5 and PTC1.0 samples with smaller mesopores (peak pore at about 2–3 nm) and larger mesopores (peak pore at around 16–18 nm). The BET surface area (S_{BET}), pore volume (V_{pore}) and pore size (d_{pore}) of the cotton, TC, PC0.5 and PTC samples are listed in Table 1, showing a totally decreasing tendency of the specific surface areas and pore volume as well as a slightly increasing average pore sizes for the PTC samples with increasing the Pt content. Two reasons possibly lead to the decreasing specific surface areas for the PTC samples with increasing the Pt content: one is the larger density of Pt than TiO_2 and cotton; another is a partial coverage of TC's surface by the Pt NPs and Na^+ from the raw materials ($NaBH_4$ and NaOH).[24] Also, compared with cotton, a significant decrease for the surface area and pore volume of PC0.5 can be observed. The surface area of PC0.5 decreased to 3.6 m^2 g^{-1} from 26.5 m^2 g^{-1} of cotton due to the similar reasons. However, the PTC0.5 sample obtained after depositing TiO_2 coating can maintain a relative high surface area (10.7 m^2

TEM image of the PTC0.25 sample, which indicates that the sizes of TiO_2 and Pt (black dots) are about 2–6 nm and 3–7 nm, respectively. The results confirm the analysis of FESEM images. With increasing the Pt loading, the size of Pt NPs increases slightly from about 3–7 nm of PTC0.25 to 5–15 nm for the PTC1.0 sample. The HRTEM image of the PTC0.25 sample (Fig. 5d) reveals that the lattice spacing of 0.224 nm can be seen, which is consistent with the lattice spacing of (111) planes of metallic Pt.[24,29] And the Pt particle size is about 4 nm.
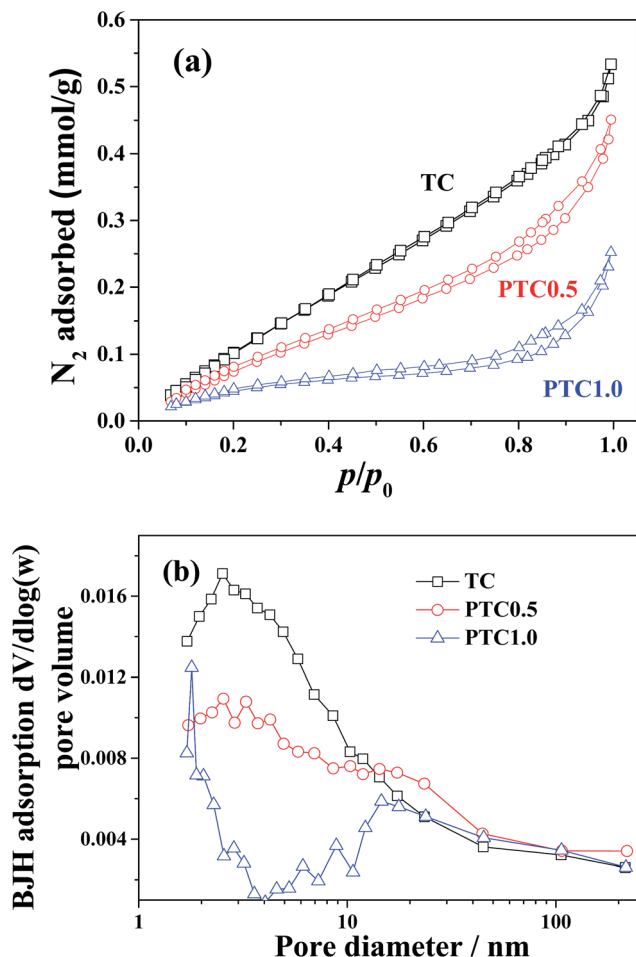
Fig. 6 Nitrogen adsorption–desorption isotherms (a) and the corresponding pore-size distribution curves (b) for the TC, PTC0.5 and PTC1.0 samples, respectively.

g^{-1}). It is worthy mentioned that the high surface area of catalyst is beneficial to the catalytic process.

3.4 XPS analysis

X-ray photoelectron spectroscopy (XPS) was used to analyze the chemical status of elements in the samples. The XPS survey spectrum (shown in Fig. 7a) of the PTC0.5 sample shows the presence of Pt, C, Ti, O and Na elements, further confirming the existence of TiO_2 coating on the surface of cotton and Pt NPs deposited on the surface of TC. Among them, sodium element comes from the residual Na^+ due to using NaOH and $NaBH_4$ as the reactants. The high-resolution Pt 4f spectra of the PTC0.25, PTC0.5 and PTC1.0 samples are shown in Fig. 7b. The two peaks located at 71.13–71.45 eV and 74.34–74.61 eV can be attributed to Pt $4f_{7/2}$ and Pt $4f_{5/2}$ of metallic Pt, respectively.[24,28] The intensities of Pt 4f peaks increase with the Pt loading. Fig. 7c reveals the high-resolution XPS spectra of Ti 2p for the PTC0.25, PTC0.5 and PTC1.0 samples. The observed two peaks at *ca.* 463.96–464.00 and 458.24–458.30 eV belong to Ti $2p_{1/2}$ and Ti $2p_{3/2}$ of Ti^{4+} in TiO_2, respectively. The high-resolution XPS spectra of O 1s for the PTC0.25, PTC0.5 and PTC1.0 samples are

shown in Fig. 7d, the fitting peaks located at 532.71–533.02 eV, 530.84–531.61 eV and 529.58–529.67 eV can be observed. The two components at 532.71–533.02 eV and 530.84–531.61 eV can be assigned to the oxygen species (O 1s) of organic O in cotton and the oxygen of the surface hydroxyl (OH) groups,[34] respectively. The peak located at 529.58–529.67 eV corresponds to the O 1s core level of the O^{2-} anions in the TiO_2.[24,34]

3.5 Evaluation of catalytic activity

A comparison of catalytic activity for the PTC0.5 and PC0.5 catalysts are shown in Fig. 8. Formaldehyde concentration/ΔCO_2 as a function of reaction time are shown in Fig. 8a and b, which show that the declined rate of HCHO concentration and the improved rate of CO_2 concentration over PTC0.5 is higher than those over PC0.5, indicating PTC0.5 is more active than PC0.5 towards HCHO oxidation.

The catalytic activity of the synthesized samples with different Pt content for HCHO oxidation was investigated (shown in Fig. 9). Fig. 9a and b show formaldehyde concentration/ΔCO_2 as a function of reaction time for the samples with different Pt content. For TC without Pt depositing, the concentration of HCHO and CO_2 decreases slightly with time, indicating the reduced HCHO was not oxidized into CO_2 but mainly adsorbed on the surface of TC. After depositing Pt on TC, the concentration of HCHO decreases and the corresponding CO_2 concentration increases, indicating that HCHO can react with O_2 to form CO_2 and H_2O at different reaction rate over the PTC catalysts with different Pt content. In the range of 0.10–0.75 wt% of Pt content, the declined rate of HCHO concentration and the improved rate of CO_2 concentration raise with increasing Pt content, indicating the increasing rate of HCHO oxidation with the Pt loading. When the Pt content further increases to 1 wt%, no obvious increase of HCHO oxidation activity is found. From the results of TEM images, the Pt particle size is slightly increases with the Pt content, indicating the number of Pt NPs and surface active Pt atoms generally increases with Pt loading in the range of 0.1–0.75 wt%. But further increasing the Pt loading to 1.0 wt%, the number of surface active Pt atoms may not have obvious increase due to the growth and aggregation of Pt NPs. At the same time, the BET surface areas of the PTC samples generally decrease with Pt loading. Therefore, combined with the results of TEM images and BET analysis, the catalytic activity increases with Pt content in the range of 0.1–0.75 wt% and no obvious increase of catalytic activity was observed when Pt content increasing to 1.0 wt%. Thus, 0.75 wt% is the optimal Pt content in view of both activity and cost.

Compared with our previous results,[31] the rates of the HCHO concentration decrease (96 ppm in 1 h) and the corresponding CO_2 concentration increase (115 ppm in 1 h) for the PTC0.25 sample (0.14 wt% real Pt content) is slightly less than those (125 ppm increase for HCHO, 181 ppm decrease for CO_2 in 1 h) for the powder-like Pt/P25 sample (0.15 wt% real Pt content) prepared in similar way in literature,[31] indicating the former is slightly less active than the latter. However, the air resistance for the PTC sample is much lower than that of the powder-like Pt/
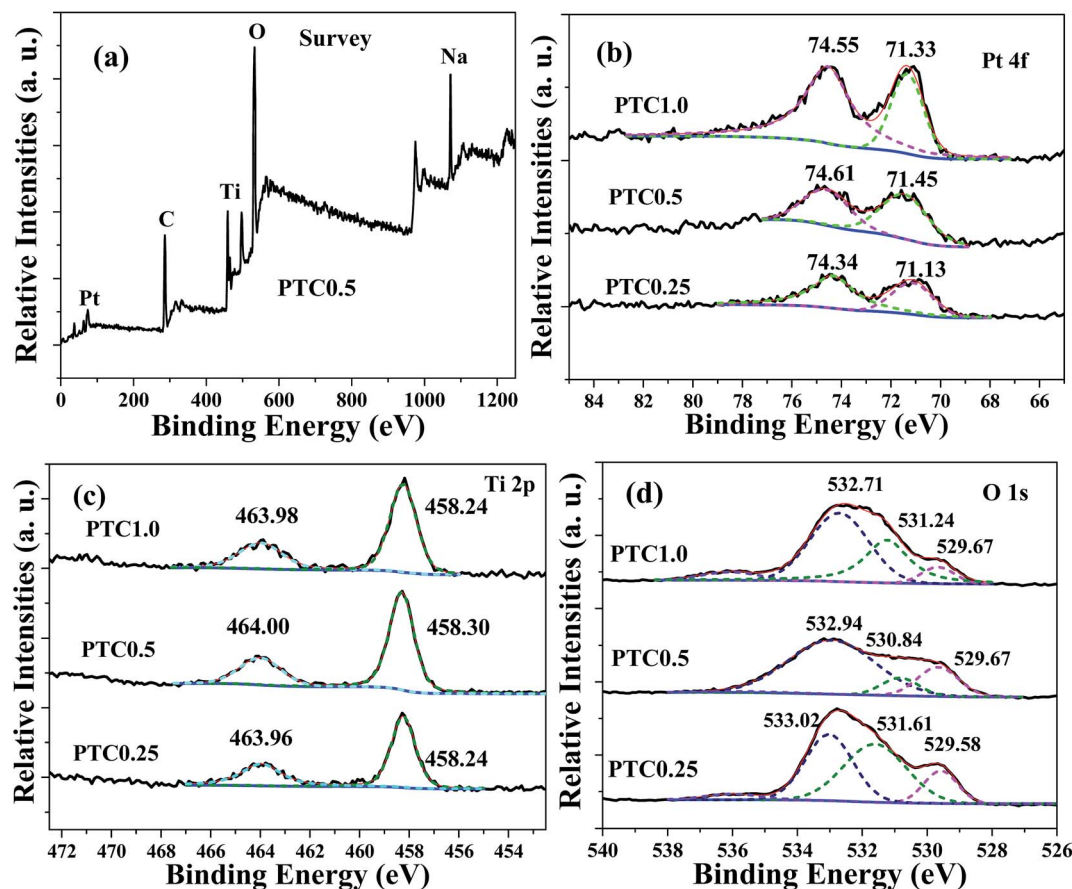
Fig. 7 Survey spectrum of the PTC0.5 sample (a), and high-resolution XPS spectra for Pt 4f (b), Ti 2p (c) and O 1s (d) of the PTC0.25, PTC0.5 and PTC1.0 samples.

P25 sample, therefore, the PTC sample is more suitable for the direct application in air purifier.

The stability of catalysts and their catalytic activity are also significant for their actual applications. For the purpose of evaluating the stability of PTC in oxidation of HCHO, the HCHO oxidation reaction over PTC0.5 was performed for four times in cycling experiments and the results are revealed in Fig. 10. It

can be seen from it that the consuming rate of HCHO (see Fig. 10a) and the generation rate of CO_2 (see Fig. 10b) over PTC0.5 in 4 repeated tests keep almost unchanged in contrast with those showed in the first-cycle, suggesting that the PTC0.5 sample exhibits a stable and good catalytic performance. Also, the stability of catalytic activity for the PC0.5 sample is also shown in Fig. S1,† which shows that an obvious declined
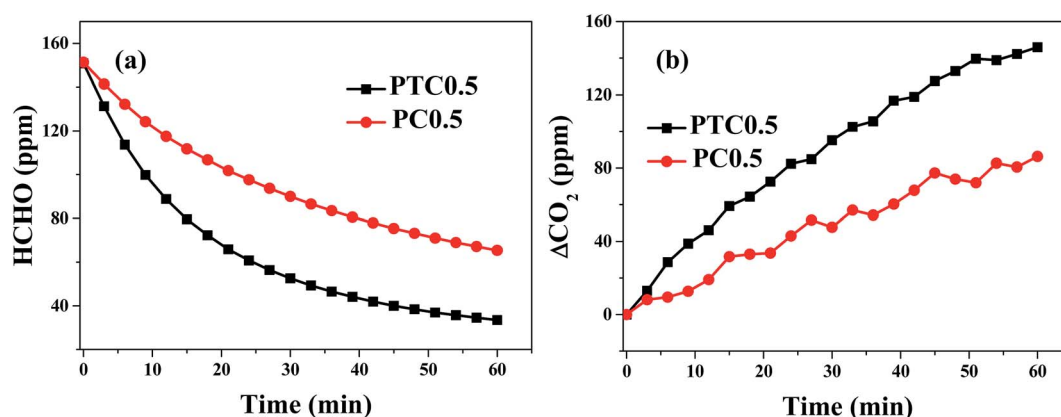

Fig. 8 Changes in formaldehyde concentration (a) and ΔCO_2 (the difference between CO_2 concentration at t reaction time and initial time, ppm) (b) as a function of reaction time for the PC0.5 and PTC0.5 samples.
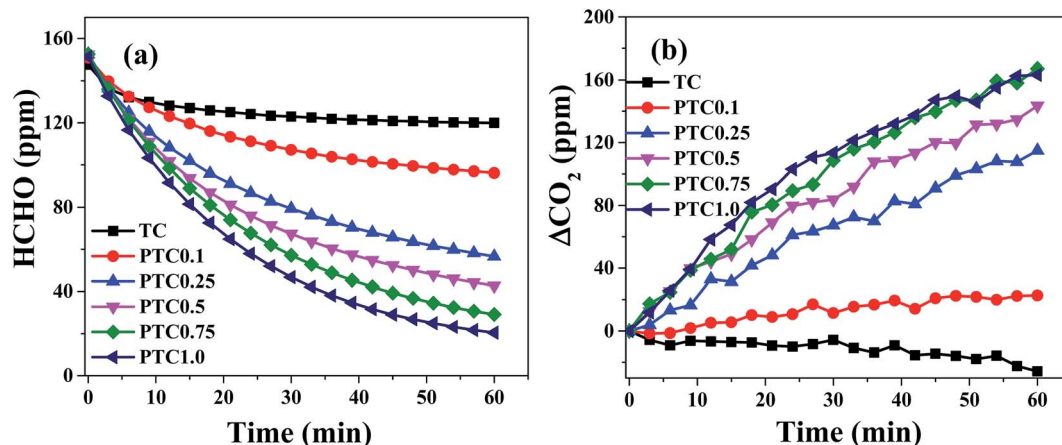
Fig. 9 Changes in formaldehyde concentration (a) and ΔCO_2 (b) as a function of reaction time for the PTC samples with different Pt content.

catalytic activity was observed for PC0.5 in repeated test (see), implying the poor stability of catalytic activity of PC0.5.

Why the PTC0.5 sample showed not only a higher catalytic activity but also a better stability compared with the PC0.5 sample? One of reasons is that the deposition of TiO_2 helps the PTC0.5 catalyst to have a relative high surface area (the surface areas are 3.6 and 10.7 $m^2 g^{-1}$ for PC0.5 and PTC0.5, respectively. See Table 1). The second reason is that, more importantly, the TiO_2 coating also benefits the activation of O_2 due to the formation of oxygen vacancies at the metal-support interface of Pt/TiO_2 (ref. 28) and the adsorption of HCHO.[24] Therefore, the TiO_2 coating in PTC catalysts plays an important role in obtaining a high catalytic activity and a good stability.

3.6 In situ DRIFTS analysis

In order to detect the intermediate species in catalytic oxidation of formaldehyde, in situ DRIFTS spectra were acquired when the PTC catalyst was exposed to mixture of HCHO + O_2 at room temperature, and the results are revealed in Fig. 11. The bands located at 3614, 3117, 2800, 2180, 1652, 1560, 1393, 1280, 1130 and 767 cm^{-1} emerged after the PTC catalyst contacted with the

mixture of HCHO + O_2. And the bands intensified gradually with the contact time in the first 30 min and then maintained a constant level after ca. 30 min. The peaks located at 1652 and 1560 cm^{-1} are attributed to the asymmetric stretching (ν_{as}) of COO of formic acid,[26,40,41] and the band at 1393 and 1280 cm^{-1} are ascribed to the symmetric stretching (ν_s) of COO of formate species.[26,42] The band located at 2800 cm^{-1} belongs to CH stretching of formate species.[27,42] The presence of about 767 cm^{-1} band further confirms the existence of formate species.[43] Furthermore, the presence of peaks at 3614 and 3117 cm^{-1} are attributed to the OH group of formate species and OH groups of water formed during the HCHO oxidation process,[27,42] respectively. A very weak band appearing at 2180 and 1130 cm^{-1} are ascribed to linear CO adsorbed on Pt[44,45] and DOM species,[46–48] respectively. The results suggest the partial oxidation of formaldehyde into DOM and further reaction with surface active O species to form formate species. No characteristic peaks related to HCHO were observed, suggesting that the complete decomposition reaction of HCHO took place on the surface of PTC, which also showed that the PTC catalyst exhibited a good catalytic activity. The results of in situ DRIFTS reveal that formic
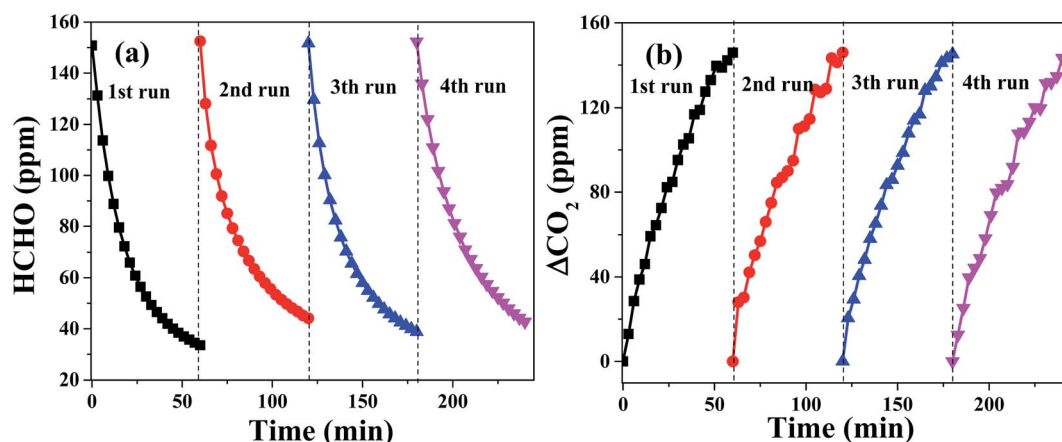

Fig. 10 Changes in formaldehyde concentration (a) and ΔCO_2 (b) as a function of reaction time for the PTC0.5 sample in four repeated tests.
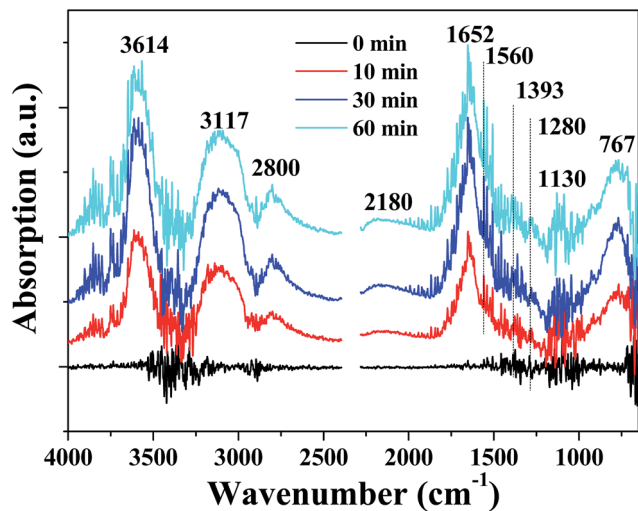
Fig. 11 *In situ* DRIFTS spectra of the PTC0.5 catalyst under a flow of HCHO/O_2 at room temperature and different reaction time.

species, CO and DOM are the main intermediate species and water is one of products during the HCHO oxidation, respectively.

3.7 Catalytic mechanism analysis

Based on the results of *in situ* DRIFTS measurement and the previous reports,[24,26,44,45,49] the schematic mechanism diagram for HCHO catalytic oxidation decomposition over PTC can be illustrated in Fig. 12. In step I, reactant molecules (HCHO and O_2) are firstly adsorbed onto the surface of PTC. Among them, HCHO molecules are adsorbed on the surface of catalyst (such as weakly bonding with H of OH groups on the surface of catalysts), which results in the positive charging of C atom of HCHO molecule. However, O_2 molecule are adsorbed on the surface of Pt NPs by chemical dissociation to form adsorbed active O atom species.[32,50] Then, adsorbed HCHO is attacked by adsorbed active O atom to form DOM species (step II) and further change into adsorbed formate species owing to the charge redistribution and molecular rearrangement (step III
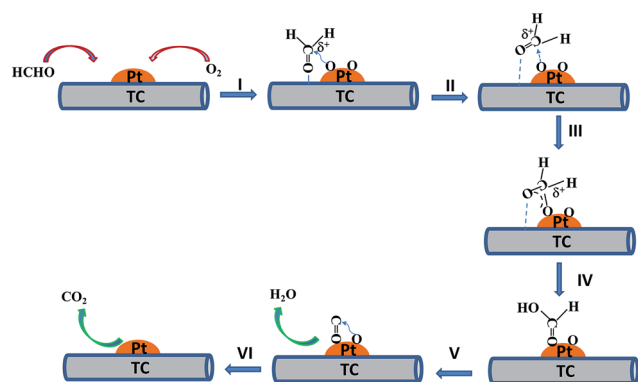
and IV). After that, the surface formate species lose one water molecule (H_2O) (step V) and the remaining adsorbed CO on the surface of Pt are further oxidized into the product of CO_2 molecule with another active O atom (step VI). In the last two steps, the product of adsorbed nonpolar CO_2 molecules can't be observed by *in situ* DRIFTS technique due to the extremely weak adsorption and fast desorption from the surface of catalysts. However, the product of adsorbed polar H_2O molecules can be observed by *in situ* DRIFTS technique due to relative strong adsorption on the surface of catalysts.

4. Conclusions

The Pt/TiO_2/cotton fiber composite catalyst was prepared by an impregnation of TiO_2/cotton fiber with Pt precursor and $NaBH_4$-reduction combined method, and HCHO can be efficiently catalytically decomposed into CO_2 and H_2O over the PTC catalyst at room temperature. The optimum Pt loading is 0.75 wt%. The PTC catalyst also exhibited good catalytic stability in recycled experiments and much lower air resistance than the powder-like sample, which is vital for its actual application. And the TiO_2 coating in PTC catalysts plays an important role in obtaining a high catalytic activity and a good stability. The formate, CO and DOM species are the main intermediate species in the catalytic oxidation of HCHO, which can be further oxidized into CO_2 and H_2O. In view of the merits of low cost and abundant raw materials for cotton, low air resistance, light mass, flexible properties and good efficiency for the PTC catalyst, this work may promote the practical application of high-performance catalysts for indoor air purification and related catalytic processes. Note that one of drawbacks of this kind of catalytic composite materials is that they are not suitable for the high-temperature reaction considering their organic supports. And more work will be done on improving the real Pt loading in catalysts in future work.

Acknowledgements

References

1 T. Salthammer, S. Mentese and R. Marutzky, *Chem. Rev.*, 2010, **110**, 2536–2572.

2 L. Nie, J. Yu, M. Jaroniec and F. F. Tao, *Catal. Sci. Technol.*, 2016, **6**, 3649–3669.

3 J. J. Collins, R. Ness, R. W. Tyl, N. Krivanek, N. A. Esmen and T. A. Hall, *Regul. Toxicol. Pharmacol.*, 2001, **34**, 17–34.

4 J. Ye, X. Zhu, B. Cheng, J. Yu and C. Jiang, *Environ. Sci. Technol. Lett.*, 2017, **4**, 20–25.

Fig. 12 Schematic mechanism diagram for HCHO oxidative decomposition over the PTC catalyst.

This journal is © The Royal Society of Chemistry 2017

5   Z. Xu, J. Yu and W. Xiao, *Chem.–Eur. J.*, 2013, **19**, 9592–9598.

6   Y. Le, D. Guo, B. Cheng and J. Yu, *Appl. Surf. Sci.*, 2013, **274**, 110–116.

7   Z. Xu, J. Yu, J. Low and M. Jaroniec, *ACS Appl. Mater. Interfaces*, 2014, **6**, 2111–2117.

8   P. Zhou, X. Zhu, J. Yu and W. Xiao, *ACS Appl. Mater. Interfaces*, 2013, **3**, 8165–8172.

9   R. C. W. Lama, M. K. H. Leung, D. Y. C. Leung, L. L. P. Vrijmoedb, W. C. Yamc and S. P. Ng, *Sol. Energy Mater. Sol. Cells*, 2007, **91**, 54–61.

10 J. Yu, S. Wang, J. Low and W. Xiao, *Phys. Chem. Chem. Phys.*, 2013, **15**, 16883–16890.

11 W. Liang, J. Li, J. Li, T. Zhu and Y. Jin, *J. Hazard. Mater.*, 2010, **175**, 1090–1095.

12 C. Zhang and H. He, *Catal. Today*, 2007, **126**, 345–350.

13 L. Liu, H. Tian, J. He, D. Wang and Q. Yang, *J. Environ. Sci.*, 2012, **24**, 1117–1124.

14 B. Liu, C. H. Hsieh, W. Wang, C. Huang and C. Huang, *Chem. Eng. J.*, 2013, **232**, 434–441.

15 H. Huang and D. Y. C. Leung, *ACS Catal.*, 2011, **1**, 348–354.

16 N. An, W. Zhang, X. Yuan, B. Pan, G. Liu, M. Jia and W. Yan, *Chem. Eng. J.*, 2013, **215–216**, 1–6.

17 Y. Huang, H. Li, M. S. Balogun, H. Yang, Y. Tong, X. Lu and H. Ji, *RSC Adv.*, 2015, **5**, 7729–7733.

18 Z. Yan, Z. Xu, J. Yu and M. Jaroniec, *Appl. Catal., B*, 2016, **199**, 458–465.

19 Z. Huang, X. Gu, Q. Cao, P. Hu, J. Hao, J. Li and X. Tang, *Angew. Chem., Int. Ed.*, 2012, **51**, 4198–4203.

20 X. Tang, Y. Li, X. Huang, Y. Xu, H. Zhu, J. Wang and W. Shen, *Appl. Catal., B*, 2006, **62**, 265–273.

21 Y. Sekine, *Atmos. Environ.*, 2002, **36**, 5543–5547.

22 J. Wang, D. Li, P. Li, P. Zhang, Q. Xu and J. Yu, *RSC Adv.*, 2015, **5**, 100434–100442.

23 J. Wang, J. Li, C. Jiang, P. Zhou, P. Zhang and J. Yu, *Appl. Catal., B*, 2017, **204**, 147–155.

24 L. Nie, J. Yu, X. Li, C. Bei, G. Liu and M. Jaroniec, *Environ. Sci. Technol.*, 2013, **47**, 2777–2783.

25 C. Zhang, H. He and K. Tanaka, *Catal. Commun.*, 2005, **6**, 211–214.

26 B. Chen, X. Zhu, M. Crocker, Y. Wang and C. Shi, *Catal. Commun.*, 2013, **42**, 93–97.

27 B. Chen, C. Shi, M. Crocker, Y. Wang and A. Zhu, *Appl. Catal., B*, 2013, **132–133**, 245–255.

28 H. Huang and D. Y. C. Leung, *J. Catal.*, 2011, **280**, 60–67.

29 L. Nie, A. Meng, J. Yu and M. Jaroniec, *Sci. Rep.*, 2013, **3**, 3215–3220.

30 L. Nie, A. Meng, F. Teng and B. Cheng, *RSC Adv.*, 2015, **5**, 83997–84003.

31 L. Nie, J. Yu and J. Fu, *ChemCatChem*, 2014, **6**, 1983–1989.

32 L. Nie, Y. Zheng and J. Yu, *Dalton Trans.*, 2014, **43**, 12935–12942.

33 M. I. Mejia, J. M. Marin, G. Restrepo, C. Pulgarin, E. Mielczarski, J. Mielczarski, Y. Arroyo, J. Lavanchy and J. Kiwi, *Appl. Catal., B*, 2009, **91**, 481–488.

34 R. Rahal, T. Pigot, D. Foix and S. Lacombe, *Appl. Catal., B*, 2011, **104**, 361–372.

35 M. Yu, Z. Wang, H. Liu, S. Xie, J. Wu, H. Jiang, J. Zhang, L. Li and J. Li, *ACS Appl. Mater. Interfaces*, 2013, **5**, 3697–3703.

36 A. Bacciarelli-Ulacha, E. Rybicki, E. Matyjas-Zgondek, A. Pawlaczyk and M. I. Szynkowska, *Ind. Eng. Chem. Res.*, 2014, **53**, 4147–4155.

37 O. L. Galkina, A. Sycheva, A. Blagodatskiy, G. Kaptay, V. L. Katanaev, G. A. Seisenbaeva, V. G. Kessler and A. V. Agafonov, *Surf. Coat. Technol.*, 2014, **253**, 171–179.

38 O. Long, L. Zheng, B. Tan and H. Shu, *Appl. Surf. Sci.*, 2016, **386**, 434–441.

39 M. Thommes, K. Kaneko, A. V. Neimark, J. P. Olivier, F. Rodriguez-Reinoso, J. Rouquerol and K. S. W. Sing, *Pure Appl. Chem.*, 2015, **87**, 1051–1069.

40 M. Calatayud, S. E. Collins, M. A. Baltanàs and A. L. Bonivardi, *Phys. Chem. Chem. Phys.*, 2009, **11**, 1397–1405.

41 Y. He and H. Ji, *Chin. J. Catal.*, 2010, **31**, 171–175.

42 Q. Xu, W. Lei, X. Li, X. Qi, J. Yu, G. Liu, J. Wang and P. Zhang, *Environ. Sci. Technol.*, 2014, **48**, 9702–9708.

43 C. J. Lavalley, J. Lamotte, G. Busca and V. Lorenzelli, *J. Chem. Soc., Chem. Commun.*, 1985, 1006–1007.

44 C. Zhang, H. He and K. Tanaka, *Appl. Catal., B*, 2006, **65**, 37–43.

45 C. Zhang, F. Liu, Y. Zhai, H. Ariga, N. Yi, Y. Liu, K. Asakura, M. Flytzani-Stephanopoulos and H. He, *Angew. Chem., Int. Ed.*, 2012, **51**, 9628–9632.

46 Z. Yan, Z. Xu, J. Yu and M. Jaroniec, *Environ. Sci. Technol.*, 2015, **49**, 6637–6644.

47 L. Qi, B. Cheng, J. Yu and W. Ho, *J. Hazard. Mater.*, 2016, **301**, 522–530.

48 B. Chen, X. Zhu, M. Crocker, Y. Wang and C. Shi, *Appl. Catal., B*, 2014, **154–155**, 73–81.

49 X. Zhu, J. Yu, C. Jiang and B. Cheng, *J. Ind. Eng. Chem.*, 2017, **45**, 197–205.

50 J. Szlachetko, D. Ferri, V. Marchionni, A. Kambolis, O. V. Safonova, C. J. Milne, O. Kröcher, M. Nachtegaal and J. Sá, *J. Am. Chem. Soc.*, 2013, **135**, 19071–19074.